SUPPLEMENTARY INFORMATION

Spectrotemporal Characterization of Photoluminescent Silicon Nanocrystals and Their Energy Transfer to Dyes

Hsin-Yun Tsai,[1] Christopher Jay T. Robidillo,[2,3] Gunwant K. Matharu,[2] Kevin O'Connor,[2] I Teng Cheong,[2] Chuyi Ni,[2] Jonathan G.C. Veinot,[2] W. Russ Algar[1,]*

[1] Department of Chemistry, University of British Columbia, 2036 Main Mall, Vancouver, British Columbia, Canada, V6T 1Z1.

[2] Department of Chemistry, University of Alberta, Edmonton, Alberta, Canada, T6G 2G2

[3] Department of Physical Sciences and Mathematics, University of the Philippines Manila, P. Faura Street, Ermita, Manila 1000, Philippines

*Corresponding author: algar@chem.ubc.ca (WRA)

Table of Contents

Supplemental Experimental Section

Materials. BHQ1 NHS ester, BHQ2 NHS ester, and BHQ3 NHS ester were from Biosearch Technologies (Teddington, UK; distributed by Cedarlane, Burlington, ON, Canada). Sulfo-cyanine 5.5 NHS ester was from Lumiprobe (Hunt Valley, MD, USA). *N*-Hydroxysuccinimide (NHS) was from Merck (Darmstadt, Germany). Sodium tetraborate decahydrate, ammonium persulfate (APS), and tetramethylethylenediamine (TEMED) were from Amresco (Solon, OH, USA). 2-(*N*-Morpholino)ethanesulfonic acid (MES), NaCl, acetic acid, NaOH, and 10× tris-borate-ethylenediaminetetraacetic acid (TBE) buffer were from Thermo-Fisher Scientific (Burlington, ON, Canada). Acrylamide:bis-acrylamide (37.5:1, 40% w/w in water) solution, Sigmacote, boric acid, agarose, 3-(trimethoxysilyl)propyl methacrylate (TMSM), Dulbecco's phosphate buffered saline (DPBS), adipic acid dihydrazide, 1-ethyl-3-(3-dimethylaminopropyl)carbodiimide (EDC), dimethyl sulfoxide anhydrous (DMSO), Amicon centrifugal filters (MWCO 30 kDa, Ultracel membrane, 0.5 mL capacity), and bovine serum were from Sigma-Aldrich (Oakville, ON, Canada). SiNCs **1** were synthesized using a previously published method.[1]

Instruments. UV-visible absorption spectra and PL emission and excitation spectra were measured with an Infinite M1000 Pro multifunction plate reader (Tecan Ltd., Morrisville, NC, USA) using a transparent half-area 96-well plate (#3679 or #3695, Corning Inc., Corning, NY, USA; or #675801; Greiner, Monroe, NC, USA) or a black 384-well plate (#3575, Corning). For absorbance measurements, the path length was 0.6 cm for sample volumes of 100 µL and 0.5 cm for volumes of 80 µL.

CGE experiments were done on an IX83 inverted epifluorescence microscope (Olympus, Richmond Hill, ON, Canada) equipped with an X-Cite 120XL metal-halide light source (Excelitas Technologies, Mississauga, ON, Canada), a high-voltage power supply (ER230; eDAQ, Colorado Springs, CO, USA), a GreenWave 16 VIS-50 portable CCD spectrometer (StellarNet, Tampa, FL, USA), and LabVIEW software (National Instruments, Austin, TX, USA). Borosilicate glass capillaries were from Drummond Scientific (75 mm length, 0.4 mm inner diameter; Drummond Scientific Co., Broomall, PA, USA). The plasma cleaner was from Harrick Plasma (PDC-32G; Ithaca, NY, USA). A glass microscope slide (75 mm × 26 mm) with a 1.3 cm-diameter centered hole was masked in

regions, coated with hydrophobic Sigmacote, and unmasked to create reservoirs at both ends for holding running buffer.

Time-resolved PL measurements were made using a sub-micro quartz cuvette (#16.100F-Q-10/Z15; Starna Cells, Inc., Atascadero, CA, USA). The excitation pluses (355 nm, 35 ps pulse duration, 10 Hz repetition, power 200−250 μJ) were generated with a Nd:YAG laser (PL2241; EKSPLA, Vilnius, Lithuania). Time-resolved PL was measured between 476−838 nm over a time range of 1 ms with an Acton spectrometer (Princeton Instruments, Trenton, NJ, USA) and a streak camera (C7700; Hamamatsu Photonics, Hamamatsu, SZK, Japan).

Estimating the Extinction Coefficient of SiNC676 1. The concentration of SiNC676 **1** was estimated from transmission electron microscopy (TEM) images and thermogravimetric analysis (TGA). The average diameter of the SiNC was determined from the TEM images, with the average mass per nanocrystal calculated from the diameter and the density of Si (2.33 g/cm^3). The quantity of Si in a SiNC676 **1** stock solution (dispersed in water) was determined by TGA, which provided the mass of Si per unit volume (mg/mL) for calculation of the SiNC concentration.

To estimate the extinction coefficient of the SiNC676 **1**, the SiNCs were dispersed in 1× DPBS to nominal concentrations of 0−14.6 μM. In total, five concentrations were prepared. Sample volumes of 100 μL were transferred into a clear-bottom half-area 96-well plate for absorbance measurements, where the path length was 0.6 cm. The absorbance at 350 nm was measured and plotted versus the nominal concentration to determine the extinction coefficient of the SiNC676 **1** (~12 160 M^{-1} cm^{-1} at 350 nm).

Note: A post-hoc revision of the nominal concentrations was later motivated by the results of energy transfer (ET) experiments with partitioned BHQ dye and modeling of a Poisson distribution with the assumption of 100% ET efficiency for one dye per SiNC (*vide infra*). The following experimental methods are written for the nominal concentration of SiNCs; however, the data in the Results sections report the revised concentrations, which are 6.7-fold larger than the nominal concentrations. There was no adjustment of the dye concentrations.

Transmission Electron Microscopy (TEM). Brightfield and darkfield images were acquired using a JEOL JEM-ARM200CF S/TEM electron microscope at an accelerating voltage of 200 kV. TEM samples were prepared by depositing a drop of a dilute toluene suspension of the sample in question onto a holey or ultra-thin carbon-coated copper grid (Electron Microscopy Sciences Inc., Hatfield, PA, USA). The prepared sample was kept in a vacuum chamber at a base pressure of 0.2 bar for at least 24 h prior to data collection. The particles size distribution was assembled as an average shifted histogram as described by Buriak *et al.* for at least 300 particles.[2]

ET Experiments with SiNC676 1 with Partitioned BHQ Dyes. Succinimidyl esters of BHQ1, BHQ2, and BHQ3 were dissolved in DMSO and the concentrations were determined by spectrophotometry using the known molar absorbance coefficients at the peak wavelengths (BHQ1: 34 000 M^{-1} cm^{-1} at 520 nm; BHQ2: 38 000 M^{-1} cm^{-1} at 570 nm; BHQ3: 42 700 M^{-1} cm^{-1} at 654 nm). The quenchers were diluted with DMSO to final concentrations of 0.012−0.50 mM, and then aliquots (0.60 nmol × n) of BHQ1, BHQ2, and BHQ3 were diluted with DMSO to final volumes of 10 μL, where n was the number of equivalents of each quencher per SiNC (0, 0.05, 0.1, 0.3, 0.5, 0.7, 1, 2, 4, and 7 eq for BHQ1; 0, 0.05, 0.1, 0.2, 0.4, 0.7, 1, 3, and 6 eq for BHQ2; 0, 0.02, 0.03, 0.05, 0.06, 0.07, 0.1, 0.15, 0.2, 0.5, 1, and 2 eq for BHQ3).

An aliquot (60 μL) of SiNC676 **1** (10 μM, 0.60 nmol, 1.0 equiv.) was added to the BHQ solutions, then 1× DPBS (330 μL, pH 7.5) was added to induce partitioning of the quenchers with the SiNCs. The final concentration of SiNCs was 1.5 μM, and the final composition of the solvent was 1× DPBS with 2.5% v/v DMSO. The samples were left at room temperature overnight and then stored at 4 °C until needed. For preparing smaller scales of samples, either 0.22 or 0.25 nmol of SiNC676 **1** was used with analogously scaled-down quantities of BHQ and DMSO.

Preparation of SiNC676 2. SiNC676 **1** (45 nmol, 1.0 equiv.) was diluted with MES buffer (0.1 M, pH 6.0, with 0.5 M NaCl) to a final volume of 510 μL. Aliquots (45 μL) of freshly prepared NHS/MES solution (200 mM, 9.0 mmol, 200 equiv.) and EDC/MES solution (200 mM, 9.0 mmol, 200 equiv.) were added to the SiNCs and let stand for 15 min at room temperature. Next, an aliquot (45 μL) of adipic acid dihydrazide (200 mM, 9.0 mmol, 200 equiv.) dissolved in 2× DPBS and an additional 2× DPBS (3.72 mL) were added, followed by mixing for 1 h at room temperature. The reaction was recharged with three additional aliquots of EDC (45 μL, 9.0 mmol, 200 equiv.) in 2× DPBS at 1 h

intervals. The final concentration of SiNC was 10 µM. The reaction was mixed overnight at room temperature, in the dark.

The reaction mixture was purified and concentrated using 30 kDa centrifugal filters (0.5 mL capacity) and spun at 14 000 RCF for 10 min. Four centrifugal filters were used in parallel and two centrifugation cycles were used for reducing the volume of the solution. The concentrated reaction mixture was then washed four times with 450 µL aliquots of 2× DPBS, spun at 14 000 RCF for 10 min. The purified SiNC **2** was further diluted with 2× DPBS buffer (~308 µL) and the final concentration was estimated via spectrophotometry using an aliquot that was diluted an additional ten-fold. The sample was stored at 4 °C until needed.

Note: A smaller scale of SiNC **2** was successfully prepared using the same procedures starting with 20 nmol of the SiNC **1** and scaled down reagent quantities.

ET Experiments with SiNC676 2 Conjugated with BHQ Dye. BHQ1 succinimidyl ester was dissolved in DMSO to final concentrations of 0.50 mM, and then aliquots (1.8 nmol × n) of the BHQ1 was further mixed with DMSO to final volume of 20 µL, where n (= 0, 1, 2, 5, 10, 20) was the desired number of equivalents of BHQ1 per SiNC676 **2**. SiNC **2** (1.8 nmol, 1.0 equiv.) was mixed with the BHQ1 solution and then 2× DPBS was added into the reaction mixture to a final volume of 180 µL. The final concentration of SiNC was 10 µM. The reaction was mixed overnight at room temperature.

Next, the reactions were diluted with 600 µL of 65% v/v EtOH (*aq*) to reduce the concentration of DMSO and the reaction mixture was concentrated using 30 kDa centrifugal filters (0.5 mL capacity) spun at 14 000 RCF for 5 min for two cycles. Purification was done using the same filters by washing seven times with 400 µL of 65% v/v EtOH (*aq*), spun at 14 000 RCF for 5 min. Then, the sample were switched to 1× DPBS using the same filters by washing four times with 450 µL of 1× DPBS, spun at 14 000 RCF for 10 min.

The volume of purified SiNC **2** was ~23 µL and 1× DPBS was added to dilute the SiNCs to a final volume of ~115 µL. The concentrations of SiNC **2** conjugated with BHQ dyes were estimated from the control reaction (n = 0) by measuring the absorbance at 350 nm. The labeling efficiencies of BHQ1 were estimated from the absorption of BHQ1 at 534 nm (absorption coefficient: 34 000 M^{-1} cm^{-1}; the

peak wavelength red-shifted from the stock solution in DMSO, presumably due to solvatochromic effects and the aqueous environment post-conjugation). Samples were diluted with 1× DPBS to final SiNC concentrations of 1.5 μM and stored at 4 °C until needed. The recovery of the SiNCs was ~43% and the labeling efficiencies for BHQ1 were between 18.7−5.8%, with lowest equivalent of BHQ1 having higher labeling efficiency.

Procedures analogous to those described above were used for labeling SiNC676 **2** with BHQ3. BHQ3 succinimidyl ester was dissolved in DMSO to final concentrations of 0.05−0.50 mM and aliquots (1.8 nmol × n) of the BHQ3 were mixed with SiNC **2**, where n (= 0, 0.06, 0.15, 0.4, 1, and 5). The labeling efficiencies of BHQ3 were estimated from the absorption of BHQ3 at 654 nm (absorption coefficient: 42 700 M^{-1} cm^{-1}; also red-shifted from the stock solution in DMSO). The recovery of the SiNCs was ~65%. The labeling efficiencies for BHQ3 were 26−9.2%.

ET Experiments with SiNC676 2 with Conjugated sCy5.5. Procedures were similar to those used to conjugate BHQ dyes. sCy5.5 succinimidyl ester was dissolved in DMSO and the concentration determined using its known absorption coefficient (211 000 M^{-1} cm^{-1} at 676 nm). Aliquots of sCy5.5 (12.4 mM, 1.8 nmol × n) were mixed with DMSO to final volumes of 20 μL, where n (= 0, 10, 20, 50) was the average equivalent of the sCy5.5 per SiNC.

SiNC676 **2** (1.8 nmol, 1.0 equiv.) was mixed with the sCy5.5 solution, and then 2× DPBS was added to a final volume of 200 μL and final SiNC concentration of 9.0 μM. The reaction was mixed overnight at room temperature. The reactions were further diluted with DPBS (600 μL) and then concentrated and purified using 30 kDa centrifugal filters (0.5 mL loading capacity) spun at 14 000 RCF for 10 min. Two centrifugation cycle were used for reducing the volume, followed by washing five times with 1× DPBS (450 μL).

The volume of purified SiNC was ~23 μL, then diluted with 1× DPBS to a final volume of ~115 μL. The concentrations of SiNC was estimated from the control reaction (n = 0) by measuring the extinction at 350 nm. The labeling efficiencies of sCy5.5 were estimated from the absorption of sCy5.5 at 676 nm. The samples were diluted with 1× DPBS to final SiNC concentrations of 1.5 μM and stored at 4 °C until needed. The recovery of the SiNC was ~57%. The labelling efficiencies for sCy5.5 were 3.1−1.0%, with lower equivalents of sCy5.5 having higher labeling efficiency.

Capillary Gel Electrophoresis. The CGE experiments were done using a small modification of previously reported protocols.[3,4]

Cleaned borosilicate glass capillaries (75 mm length, 0.4 mm inner diameter) were immersed in TMSM/acetic acid/ethanol solution (3% v/v TMSM, 1% v/v acetic acid) for 4 h. The TMSM-modified capillaries were dried in air and heated at ~70 °C overnight. To form a 3.0% w/w gel, acrylamide:bis-acrylamide solution (37.5:1, 40% w/w in water, 113 µL) was diluted with borate buffer (50 mM, pH 8.6 or 9.2, 1381 µL), then TEMED (neat, 1.5 µL) and APS solution (4.5 µL, 25% w/v in water) were added to the solution. The TMSM-modified capillaries were filled with the gel precursor solution by capillary action and left at room temperature for 2−3 h. The gel-filled capillaries were soaked and stored in borate buffer until needed.

The gel-filled capillaries were truncated to ~5.5 cm to fit in the custom gel electrophoresis setup. The concentration of SiNC **1** in samples was ~6.4 µM or ~182 µM and fluorescein (~30 nM or ~1.5 µM) was added as an internal standard. The SiNC samples (SiNC717 **1** or SiNC605 **1**) were electrokinetically injected into capillaries by applying 300 V for 5 s. The running buffer was borate buffer (50 mM, pH 9.2) and the field strength was ~55 V/cm (300 V was applied across the two electrodes). The setup was mounted on an IX83 inverted microscope (Olympus, Richmond Hill, ON, Canada) equipped with a metal-halide light source, excitation filter (405/20 nm for SiNC717 or 380/15 nm for SiNC605; center wavelength/bandwidth), dichroic mirror (510 nm or 425 nm cutoff), and emission filter (530 nm or 435 nm longpass). A CCD spectrometer was connected to the microscope via an optical fiber to record PL spectra during the electrophoresis. The PL data were recorded using a custom LabVIEW program with a 2 s interval and a 0.8 s detector integration time.

Slab Gel Electrophoresis. A 0.5% w/v agarose gel was prepared with TBE buffer (89 mM Tris base, 89 mM boric acid, 2 mM EDTA, pH 8.3). The SiNC676 **1** and SiNC676 **2** were individually dispersed in 2× DPBS to a final volume of 16.8 µL and an aliquot (4.2 µL) of 50% v/v glycerol (*aq*) was added. Samples of SiNC (20 µL, ~30 pmol) were loaded into wells and the gels were run at ~6.7 V/cm for 30 min in TBE buffer. The gel was illuminated with a 302-nm wavelength excitation source and imaged with a Gel Doc XR+ Imager (Bio-Rad, Mississauga, ON, Canada).

Measurements of PL Spectra. PL emission and excitation spectra were measured using the settings summarized in Table S1 (next page). Delay times and integration times for TG measurements were as specified in figures and figure captions.

Fitting Spectra. The PL emission spectra of SiNC676 **1**, SiNC676 **1** partitioned with BHQ dyes, SiNC676 **2**, and SiNC676 **2** conjugated with BHQ dyes were fit with a GCAS function (Gram-Charlier peak function) to determine peak PL emission wavelengths and the FWHM of the emission peaks. The Pl emission spectra acquired with a 2000 μs integration time were used for calculating quenching efficiencies.

Since the PL emission spectra of the SiNC and sCy5.5 overlapped, spectral unmixing was required to resolve the separate contributions from each emitter. The isolated SiNC was contribution was required for estimating the SiNC quenching efficiency due to ET with conjugated with sCy5.5. First, the sCy5.5 emission spectrum (measured in the absence of SiNC) was fitted with two bigaussian functions, where the fit parameters (*e.g.* central wavelengths, peak widths, ratio of peak heights) were recorded. Next, the emission spectra of SiNC676 **2** with conjugated sCy5.5 (2000 μs integration time) were fitted with three bigaussian functions. Two of these functions were pre-set to the fit parameters for sCy5.5 while still allowing for fitting a change in amplitude. The parameters of the third bigaussian function were left flexible for fitting to the emission contribution of the SiNC.

Table S1. Wavelength parameters and sample information for measurements of PL spectra.

Figure(s)	Material	Conc. (µM)	Buffer	Vol. (µL)	Plate	Excitation λ/Bandwidth (nm)	Emission λ/Bandwidth (nm)
3B−C, S3B	SiNC 717 **1**	~6.4	Borate	100	96-well	280/2.5	400−850/5
S3C	SiNC 717 **1**	~6.4	Borate	100	96-well	230−300/2.5 301−702/5	712/5
S4	SiNC 717 **1**	~6.4	Borate	100	96-well	252−300/2.5 300−600/5 (12-nm increment)	450−846/5 (12-nm increment)
S5B	SiNC 605 **1**	~12.6	Borate	100	96-well	280/2.5	400−850/5
S5C	SiNC 605 **1**	~12.6	Borate	100	96-well	230−300/2.5 301−500/5	582/5
S6	SiNC 605 **1**	~12.6	Borate	80	96-well	230−300/2.5 301−636/5 (14-nm increment)	349−839/5 (14-nm increment)
1C, 5A, 6, 7B, S12, S13B, S14, S15	SiNC676 **1** partitioned with BHQs	1.5	1× DPBS with 2.5 % DMSO	100	96-well	240/2.5	400−850/5
1C	SiNC676 **1** partitioned with BHQs	1.5	1× DPBS with 2.5 % DMSO	100	96-well	240−300/2.5 301−660/5	672/5
8, S17, S18, S19	SiNC676 **2** conjugated with BHQs	1.5	1× DPBS	100	96-well	240/2.5	400−850/5
9	SiNC676 **2** conjugated with sCy5.5	1.5	1× DPBS	100	96-well	240/2.5	400−850/5
S10	SiNC676 **1** partitioned with BHQs	1.5 or 0.89	1× DPBS with 2.5% DMSO or with 41.5% DMSO	100	96-well	240/2.5	400−850/5
10	SiNC676 **2** conjugated with sCy5.5	0.75	50% serum	40	384-well	240/4	400−850/5

BHQ Dissociation Test. SiNC676 **1** (1.5 µM) partitioned with BHQ dyes was prepared as described earlier. Briefly, the SiNC676 **1** (0.25 nmol, 1.0 equiv.) were mixed with 1.0 equivalents of BHQ1, BHQ2, and BHQ3 individually. SiNCs without quenchers were prepared and used as reference samples. Sample volumes of 100 µL of the SiNC676 **1** and SiNC676 **1** partitioned with BHQ samples (in 1× DPBS with 2.5% v/v DMSO) were transferred into a 96-well black plate for PL measurement, and the integrated PL intensities were used for calculating the quenching efficiencies caused by adsorption of the quenchers. Another 63 µL aliquot of the SiNC from each sample was mixed with 42 µL of DMSO individually to allow the quenchers to dissociate from the SiNCs. The final concentration of SiNC was 0.89 µM, and the final composition of the solvent was 1× DPBS with 41.5% v/v DMSO. Aliquots (100 µL) of these SiNC samples were transferred into a 96-well black plate for PL measurements, and the integrated PL intensities were used to calculate the quenching efficiencies caused by putative solvent-induced dissociation of the quenchers.

Preparation of Serum Samples. SiNC676 **2** and SiNC676 **2** with conjugated sCy5.5 were dispersed in 1× DPBS at a final concentration of 1.5 µM. An aliquot (25 µL) of the SiNCs was mixed with 25 µL of bovine serum, from which 40µL was transferred into a 384-well black plate for PL measurements.

Quantum Yield Measurement. The quantum yields of SiNC676 **1** and SiNC676 **2** were estimated by comparison to the quantum yield of fluorescein, using a procedure adopted from previous reports with minor modifications.[5,6] The fluorescein was dissolved in 0.1 N NaOH (*aq*) where it has a reported quantum yield (Φ_{FL}) of 0.91.[7,8] The SiNC samples were dispersed in 1× DPBS. Series of dilutions of fluorescein and SiNCs were prepared. The extinction values at 240 nm were measured, and emission spectra were measured with 240 nm excitation. The integrated PL intensities were plotted (500−850 nm) as functions of the extinction values, and linear fits were applied with a constraint that intercept at y = 0. To have reliable fluorescein absorbance values without saturated PL signals, the absorbance values of fluorescein samples were obtained from their 10-fold more concentrated samples, such that the absorbance values for samples used for fluorescence measurements was obtained by dividing by this dilution factor. The quantum yields of SiNCs were obtained from the slopes (I_{SiNC}/A_{SiNC}) of the plots, where I_{SiNC} is the integrated PL intensity, A_{SiNC} is extinction at the excitation wavelength, and n_{SiNC} and n_{FL} are the refractive index of the solvents (~1.334 for both).

$$\Phi_{SiNC} = \Phi_{FL} \frac{I_{SiNC}}{A_{SiNC}} \frac{A_{FL}}{I_{FL}} \frac{n_{SiNC}^2}{n_{FL}^2} \tag{S1}$$

The quantum yields estimated this message are likely to have some negative bias, as Eqn. S1 requires an absorbance but what was practically measured for the SiNCs was extinction (*i.e.* scattering + absorbance). Measurements with an integrating sphere would not have this bias. Nevertheless, the estimated quantum yield values are likely to be sufficiently accurate for estimating Förster distances and consequences for FRET.

Calculation of FRET Parameters. The Förster distances (R_0, in nm) were calculated using Eqn. S2, where κ^2 was the orientation factor (generally assumed to be 2/3), Φ_D was the quantum yield of the FRET donor (SiNC676 **1**), n was the refractive index of the solvent (1.334), and J was the spectral overlap integral. The J (in mol^{-1} cm^{-1} nm^4) was calculated using Eqn. S3, where λ (in nm) was the wavelength, $I_D(\lambda)$ was the PL intensity of the FRET donor at λ nm, $\varepsilon_A(\lambda)$ (in M^{-1} cm^{-1}) was the absorbance coefficient of the FRET acceptor at λ nm. The $J(\lambda)$ (in mol^{-1} cm^{-1} nm^4) was the spectral overlap function calculated using Eqn. S4.

$$R_0 = 0.02108(\kappa^2 \Phi_D n^{-4} J)^{1/6} \tag{S2}$$

$$J = \frac{\int I_D(\lambda)\varepsilon_A(\lambda)\lambda^4 d\lambda}{\int I_D(\lambda)d\lambda} \tag{S3}$$

$$J(\lambda) = \frac{I_D(\lambda)\varepsilon_A(\lambda)\lambda^4}{\int I_D(\lambda)d\lambda} \tag{S4}$$

Post-hoc Correction of SiNC Concentrations. The most efficient ET possible is 100% quenching of an SiNC when only one BHQ dye is associated with it. Plotting the experimentally measured ET efficiency versus the number of equivalents of BHQ (*e.g.* Fig. 6B) yielded ET efficiencies that were unrealistically high when the number of equivalents was derived from nominal concentration of SiNCs. That is, efficiencies were higher than the fraction of SiNCs that would have at least one associated BHQ dye. Since the number of dyes per SiNC was expected to follow a Poisson distribution across the ensemble, the following method was used for post-hoc correction of the BHQ/SiNC ratio:

- Assume one partitioned BHQ3 per SiNC results in 100% efficient ET, and that the partition equilibrium very strongly favors association between BHQ3 and SiNC.
- Use Poisson statistics to determine the number of equivalents of BHQ3 that would yield a fraction of SiNCs with ≥ 1 associated BHQ3 that is equal to an experimentally measured ET efficiency for partitioned BHQ3.
- For each measured ET efficiency, compare the Poisson-calculated number of equivalents to the nominal number of equivalents and calculate the ratio between the two values.
- Average the ratios across all measured ET efficiencies for partitioned BHQ3.

The result was a correction factor of 6.7 (*i.e.* an apparent concentration of SiNCs that was 6.7-fold lower than the nominal concentration).

It was not practical to apply this process with BHQ1 and BHQ2. For BHQ1, the smaller FRET-relevant spectral overlap and shorter Förster distance resulted in large numbers of dye equivalents being needed to reach high FRET efficiencies. These high numbers would limit the precision of the statistics and make it less valid to ignore partition equilibria that may have less than 100% dye associated with SiNC. For BHQ2, the formation of H-dimers confounded isolation of the FRET process, making the process unreliable.

The 6.7-fold correction derived for BHQ3 was applied to all numbers of dye equivalents plotted in the main text and in the SI, whether BHQ1, BHQ2, BHQ3, or sCy5.5.

Supplemental Results and Discussion

TEM Analysis. TEM images were used to analyze the size distribution of SiNC676 **1**. The average diameter was 4.2 ± 1.1 nm, estimated from 313 nanocrystals (Figure S1).[2]
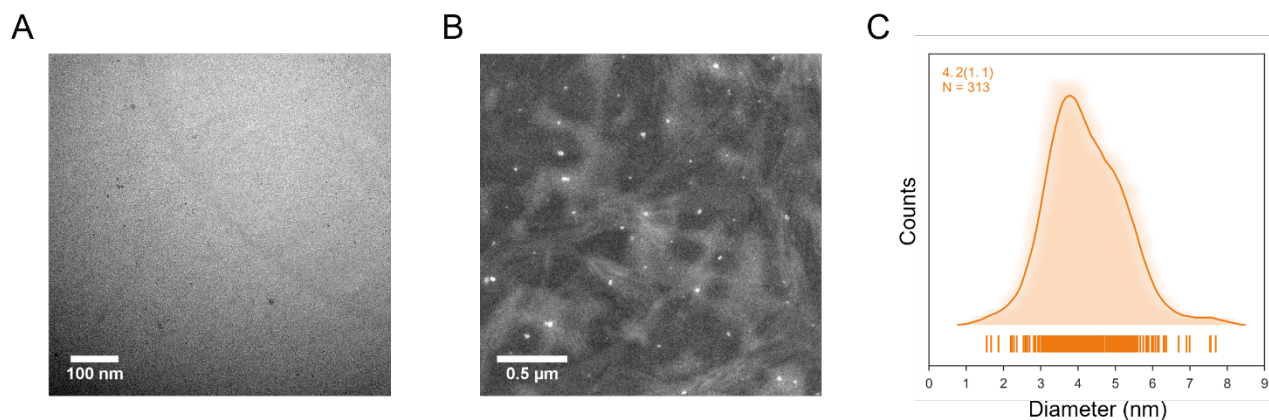

Figure S1. TEM analysis of SiNC676 **1**. **(A)** Brightfield TEM image of SiNC676 **1**. **(B)** Dark field TEM image of SiNC676 **1**. **(C)** An average shifted histogram[2] showing the size distribution of SiNC676 **1** measured from TEM images.

Spectroelectrophoresis of SiNC605 1. PL electropherograms of SiNC605 **1** were acquired at wavelengths between 530–710 nm. The peak emission wavelength increased as the migration time increased (Figure S2A). In turn, the emission spectrum gradually red-shifted by ~80 nm as the migration time increased (Figure S2B−C). These data revealed size polydispersity in the population of SiNC605 **1**, where larger SiNCs had longer emission wavelengths on average, consistent with expectations from quantum confinement.
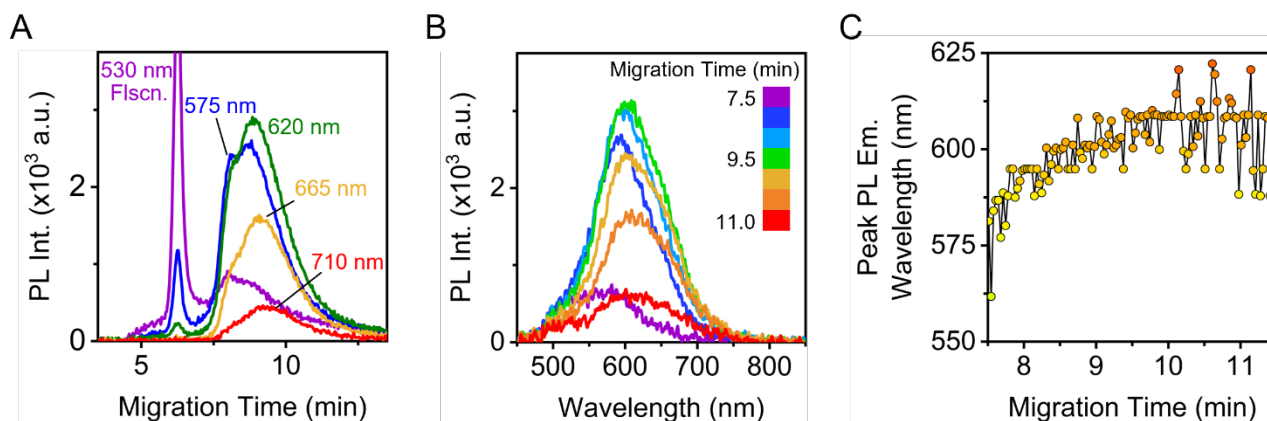
Figure S2. Spectroelectrophoresis of SiNC605 **1**. **(A)** PL electropherograms measured at different emission wavelengths. PL emission measurements were made with continuous (not pulsed) excitation. The electropherograms include a peak for a fluorescein (Flscn.) as an internal standard. **(B)** PL emission spectra as a function of migration time for the same experiment as panel A. **(C)** Plot of the peak PL emission wavelength versus migration time.

Extinction and TG Emission/Excitation Spectra and EEMs of SiNC717 and SiNC605. Figure S3A shows the extinction spectrum of SiNC717 **1**. Figure S3B shows that the emission peak of SiNC717 **1** shifted to longer wavelengths and decreased in intensity as the delay time increased. In contrast, Figure S3C shows the excitation spectra did not shift with delay time, although the intensity still decreased as the delay time increased. Figure S4 shows the time-gated EEMs of SiNC717 **1** for integration times of 2000 µs and 20 µs. The delay times varied between 0−300 µs. Analogous results for SiNC605 are shown in Figures S5–S6 and show analogous trends.
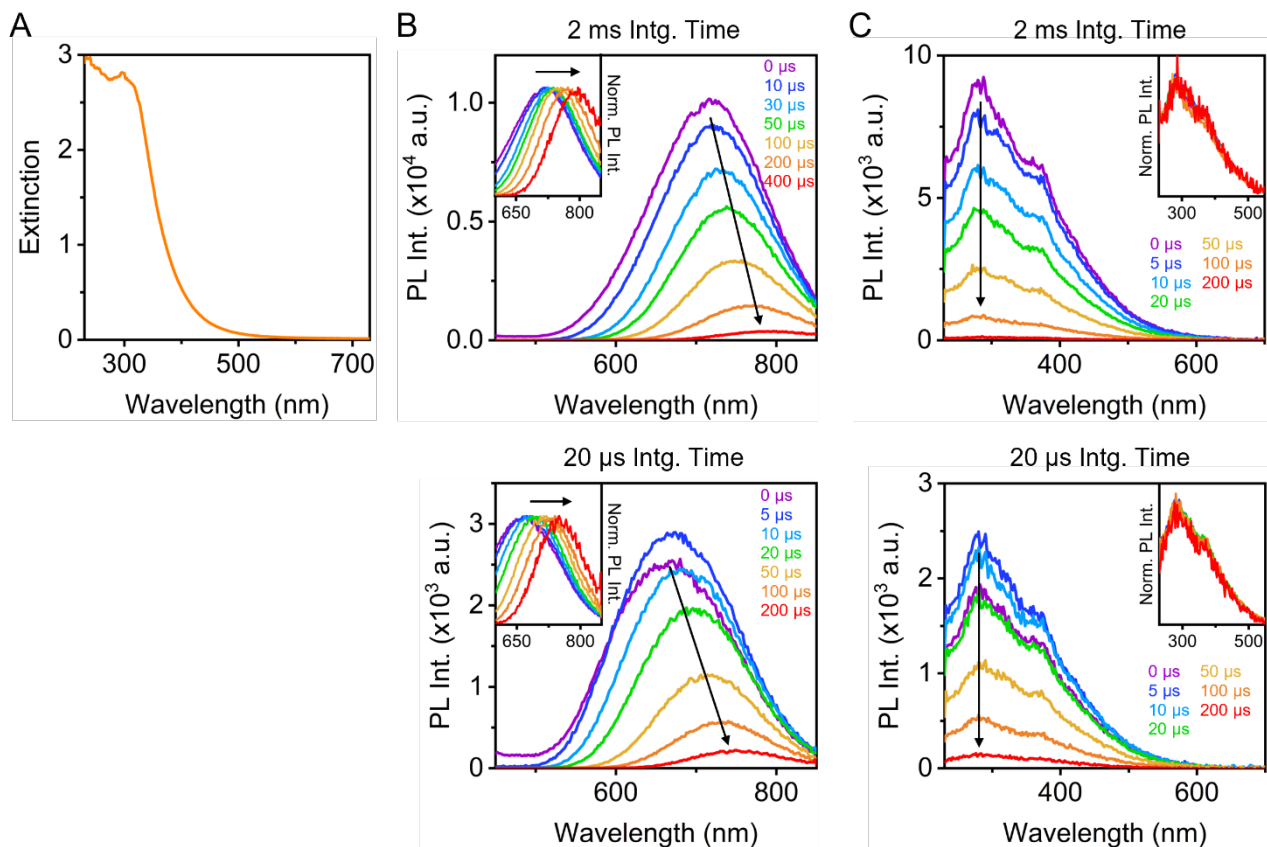
Figure S3. Spectra characterization of SiNC717 **1**. **(A)** Extinction spectrum. **(B)** PL emission spectra with (i) various delay times and 2000 µs integration time, and (ii) various delay times and 20 µs integration time. **(C)** PL excitation spectra with (i) various delay times and 2000 µs integration time, and (ii) various delay times and 20 µs integration time.
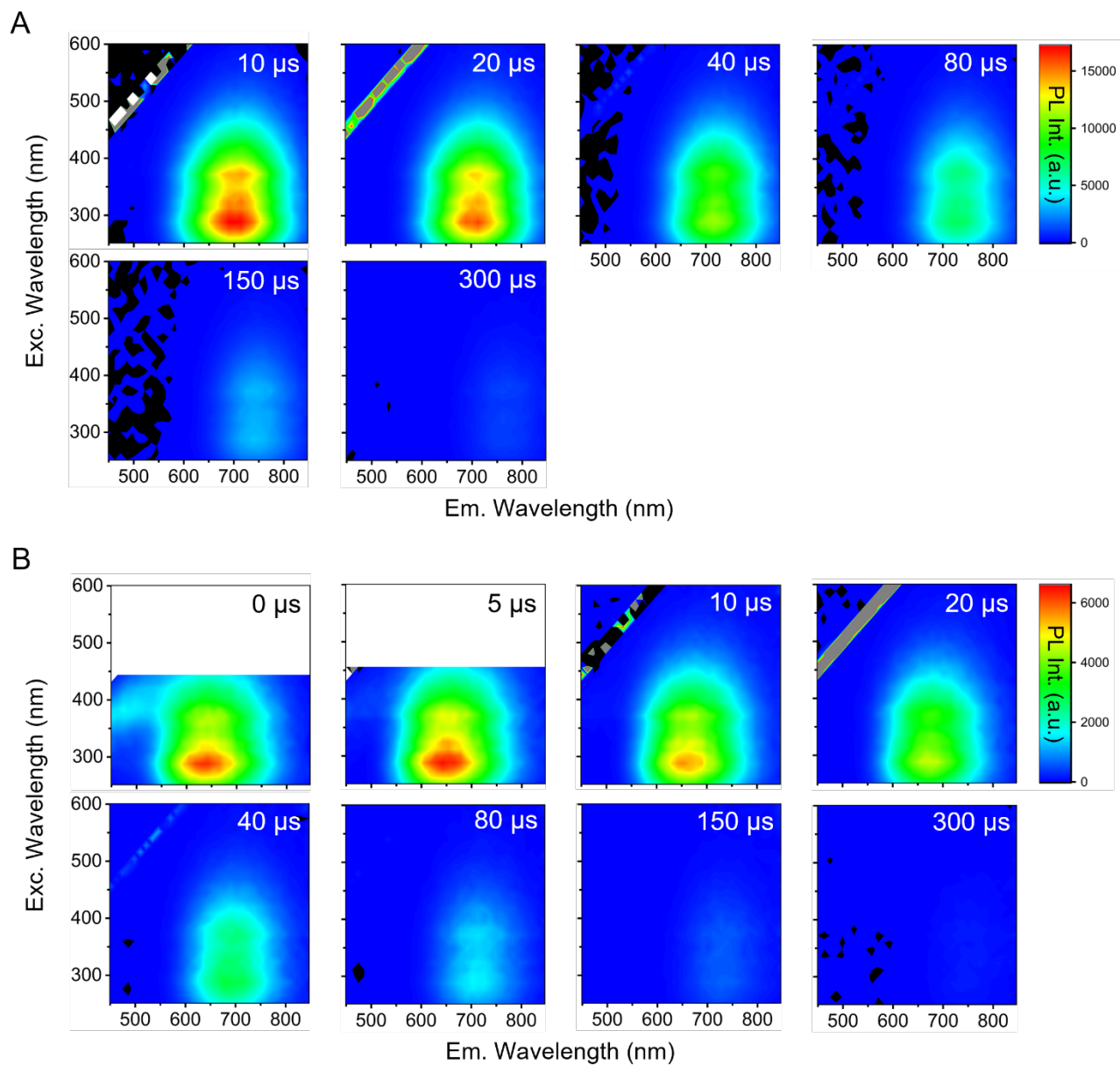
Figure S4. Time-gated EEMs of SiNC717 **1**: **(A)** various delay times with a fixed 2000 μs integration time; **(B)** various delay times with a fixed 20 μs integration time.
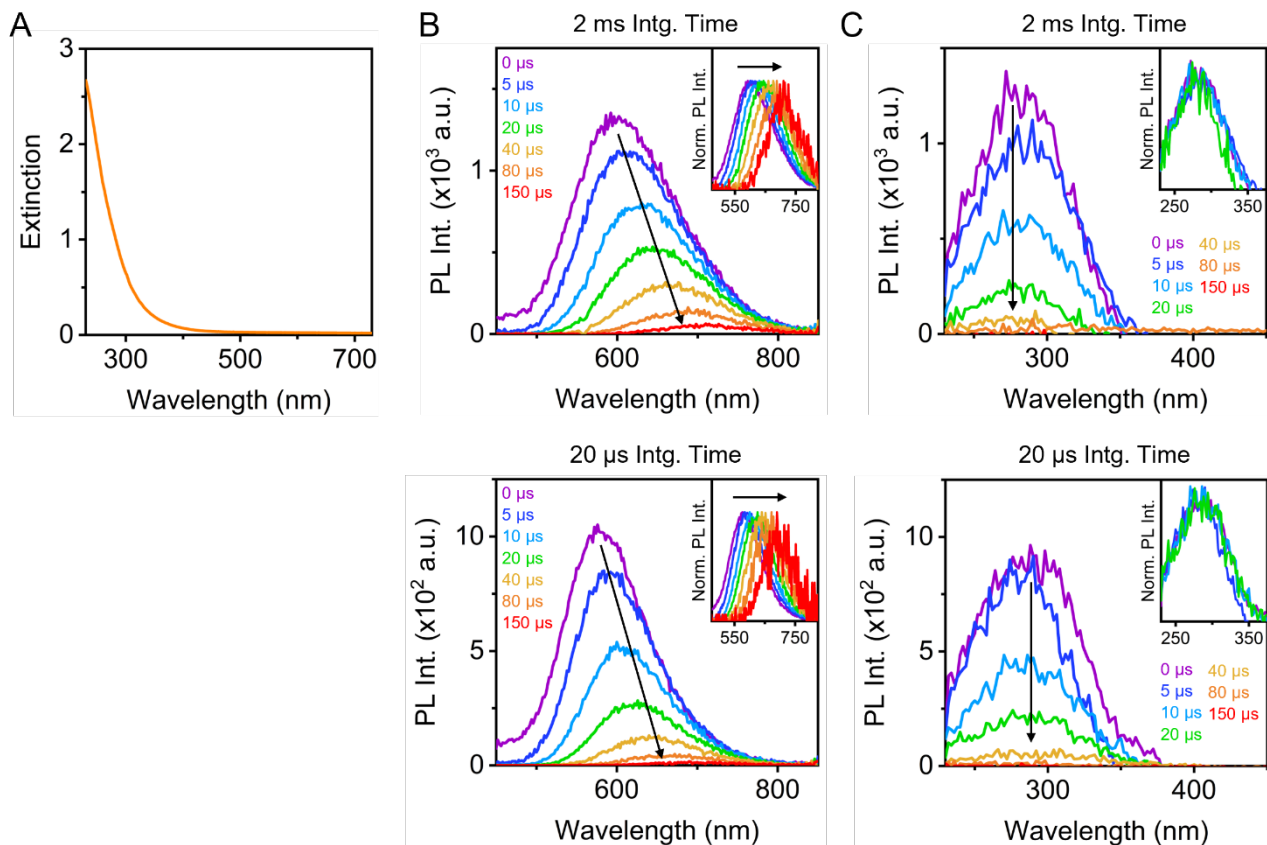
Figure S5. Spectra of SiNC605 **1**. **(A)** Extinction spectrum. **(B)** Emission spectra with (i) various delay and 2000 µs integration time, and (ii) various delay and 20 µs integration time. **(C)** Excitation spectra with (i) various delay and 2000 µs integration time, and (ii) various delay and 20 µs integration time.
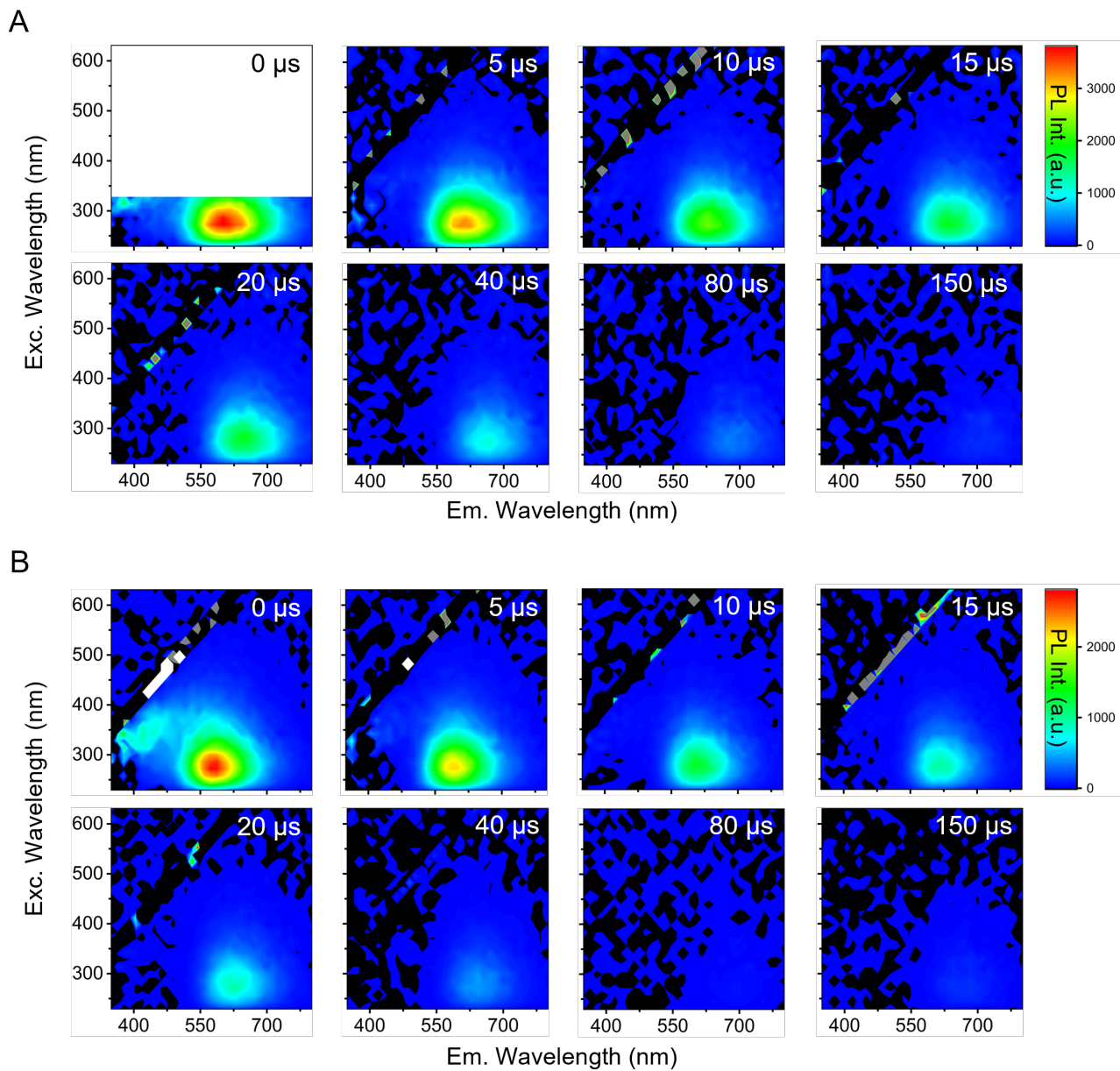
Figure S6. Time-gated EEMs of SiNC717 **1**: **(A)** various delay times with a fixed 2000 μs integration time; **(B)** various delay times with a fixed 20 μs integration time.

Estimated Extinction Coefficient of SiNC676 1. The concentration of SiNC676 **1** was estimated by combining the results of TGA and TEM analysis (see pg. S-4, for details). The extinction coefficient of SiNC676 **1** was estimated from a plot of the nominal absorbance values versus the concentration. The slope of the linear fit (12 160 M^{-1} cm^{-1}) was the extinction coefficient at 350 nm.
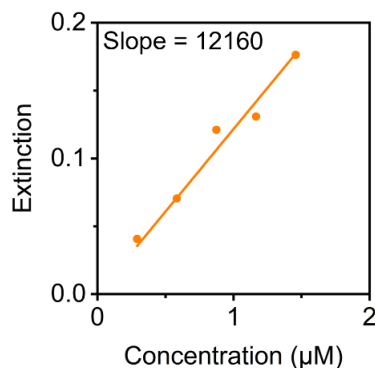

Figure S7. Nominal absorbance values (350 nm, 1 cm path length) versus the concentration of SiNC676 **1**.

Note: Concentrations were ultimately revised based on results from FRET experiments (see pg. S-4 and S-13) and reported on this basis rather than the estimated extinction coefficient.

Quantum Yield of SiNC676 1 and 2. The quantum yields of SiNC676 **1** and SiNC676 **2** were estimated by comparison to the quantum yield of fluorescein. Integrated PL intensities were plotted as function of the absorbance at the excitation wavelength. Linear fits were applied with constraining the y-intercept to a value of zero. The slopes of the linear fits were proportional to their quantum yield. The quantum yield of the fluorescein reference is reported as 0.91, and the quantum yield of SiNC676 **1** and SiNC676 **2** were 0.086 and 0.029, respectively.
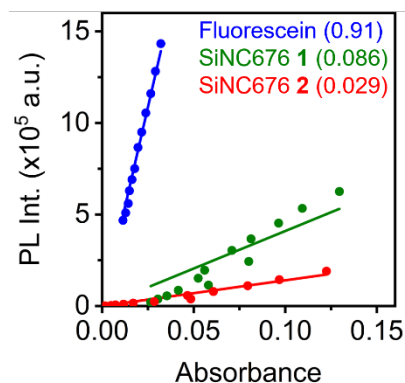

Figure S8. Plot for estimating the quantum yield of SiNC676 **1** and SiNC676 **2** using fluorescein as a standard.

Tests for Partitioning of BHQ Dyes and Inner Filter Effects. SiNC676 **1** were mixed with 0, 33, and 67 equivalents of BHQ1 (1× DPBS with 2.5% v/v DMSO). Dye that was not associated with the SiNCs were removed via centrifugal filtration (30 kDa MWCO). After first cycle of centrifugation, the SiNC samples were redispersed in 1× DPBS with 2.5% v/v DMSO (450 μL) and another cycle of centrifugation filtration was done. The filtrates were collected separately and the absorption spectra of each was measured. Figure S9 shows that the spectra lacked an absorption feature for BHQ1, consistent with most of the BHQ1 being partitioned onto the surface of SiNC676 **1**.
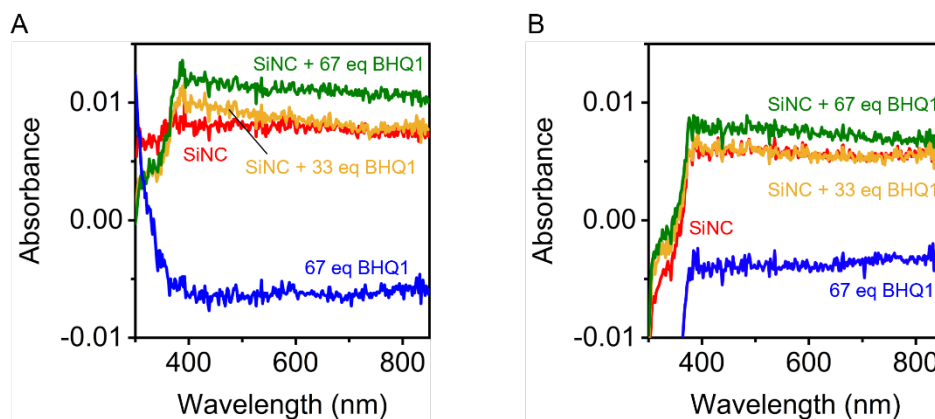

Figure S9. Filtrates of SiNC676 **1** and SiNC 676 **1** partitioned with BHQ1 samples. **(A)** Absorption spectra of filtrates collected from first cycle of spin filtration. **(B)** Absorption spectra of filtrates collected from second cycle of spin filtration.

In another experiment, SiNC676 **1** were separately mixed with 1.0 equivalents of BHQ1, BHQ2, and BHQ3. Figure S10A shows the PL emission spectra of SiNC676 1 with partitioned BHQ dyes. Compared to control sample without BHQ, the SiNC PL intensity was quenched with apparent ET efficiencies of 63%, 38%, and 98% for BHQ1, BHQ2, and BHQ3, respectively. After adding DMSO to the samples (final concentration 41.5% v/v), the ET efficiencies decreased to 10%, 3.3%, and 26% for BHQ1, BHQ2, and BHQ3, respectively (Figure S10B). Since DMSO is a much better solvent for the BHQ, dissociation of the dyes from the SiNC was expected. This dissociation would not alter inner filter effects but would result in loss of ET. These results therefore suggested the main contribution to quenching of SiNC PL by BHQ dyes was ET rather than inner filter effects. Although there was some DMSO-induced quenching of SiNC, the control sample should have largely accounted for this behavior.
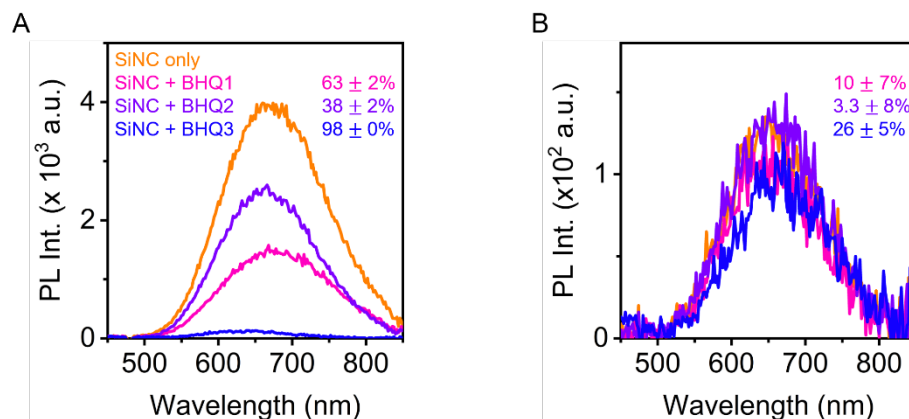
Figure S10. BHQ dissociation test. **(A)** Before adding a significant amount of DMSO, BHQ dyes are partitioned within the surface coating of the SiNCs. ET occurs from the SiNCs to the BHQ dyes, resulting in quenching of the SiNCs. **(B)** After adding DMSO to final concentration of 41.5% v/v, the BHQ dyes largely dissociate from the surface of SiNCs and the quenching was significantly reduced.

Additional Data for SiNC676 1 Partitioned with BHQ1, BHQ2, and BHQ3 Dyes. The absorption spectra of SiNC676 **1** partitioned with variable equivalents of BHQ1, BHQ2, and BHQ3 samples were measured (Figure S11A). For all but two samples (47 equiv. of BHQ1, 40 equiv. of BHQ2), the peak absorbance values for the BHQ1, BHQ2, and BHQ3 absorption peak were $\lesssim 0.1$, suggesting that inner filter effects would be minor.
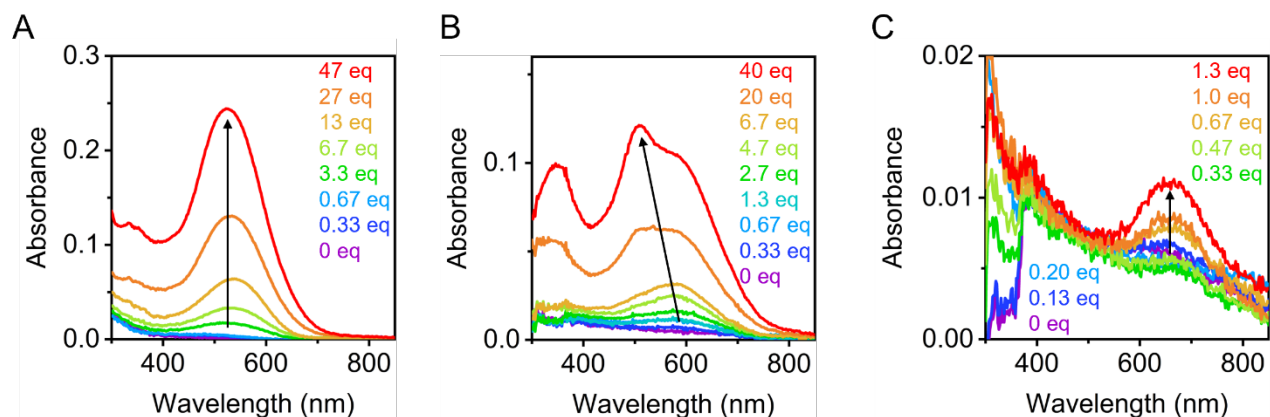

Figure S11. Absorption spectra of SiNC676 **1** partitioned with different equivalents of **(A)** BHQ1, **(B)** BHQ2, and **(C)** BHQ3 dye.

The shift in the PL emission spectrum (0 μs delay, 2 ms integration time) of SiNC676 **1** with partitioned BHQ2 was monotonically hypsochromic as the number of equivalents of BHQ2 increased (Figure S12A). The wavelength-dependent quenching efficiency with partitioned BHQ2 was higher at longer wavelengths (Figure S12B).
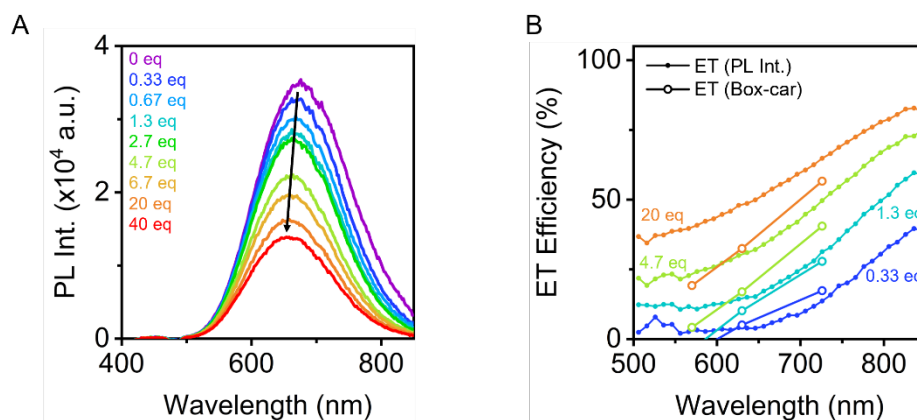

Figure S12. SiNC676 **1** with various equivalents of partitioned BHQ2: **(A)** Emission spectra (0 μs delay, 2000 μs integration time); **(B)** ET efficiency measured as a function of wavelength from the PL intensity data in panel A (solid points) and from PL lifetimes (box-car method; hollow points; see Figure S13).

PL lifetimes were analyzed for three wavelength windows: 540−600 nm, 600−660 nm, and 696−756 nm. The PL lifetime was longest in the long wavelength window and decreased with an increasing number of equivalents of partitioned BHQ2 (Figure S13A). PL decays obtained by the box-car method (Figure S13B) had the same trends. The ET efficiencies derived in the three wavelength windows using the box-car method (Figure S13B) increased as wavelength increased, similar to the PL intensity data (Figure S12B).
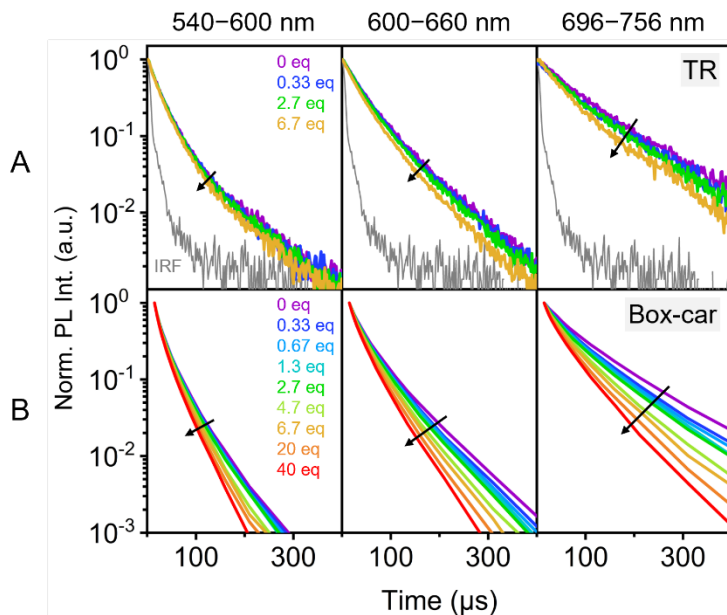
Figure S13. PL lifetime measurements of SiNC676 **1** partitioned with BHQ2. **(A)** TR PL decay of SiNC676 **1** with various equivalents of partitioned BHQ2 for wavelength ranges of 540−600 nm, 600−660 nm, and 696−756 nm. **(B)** Box-car measurements for 540−600 nm, 600−660 nm, and 696−756 nm.

Another set of SiNC PL emission spectrum measurements were done with a variable delay time and fixed 20 µs integration time to obtain "spectral snapshots" biased toward different sizes of SiNC. As already established, the peak PL wavelength bathochromically-shifted with increasing delay time for the SiNC alone (Figure S3Bii and S5Bii). With BHQ1, the temporal trajectory for the peak SiNC676 **1** PL wavelength had a gradual bathochromic shift (up to 45 nm) with increasing equivalents of dye. The FWHM changed from a trajectory that narrowed by 7 nm to one that widened up to 30 nm (Figure S14Aii). In contrast, with BHQ3, the gradual temporal shift in the trajectory for the peak PL wavelength was smaller and hypsochromic, and the FWHMs narrowed with a slightly faster rate of narrowing with more equivalents of dye (Figure S14C). These shifts in the spectral trajectories were consistent with the shifts observed in the prompt spectra and more efficient ET between smaller SiNCs and BHQ1 and between larger SiNCs and BHQ3. For samples with partitioned BHQ2 (Figure S14B), the temporal trajectory for the peak shift and FWHM were similar to those observed with BHQ3. The gradual temporal shift in the trajectory for the peak PL wavelength was small and hyposochromic, and the FWHMs narrowed at a slightly faster rate with more equivalents of BHQ2.
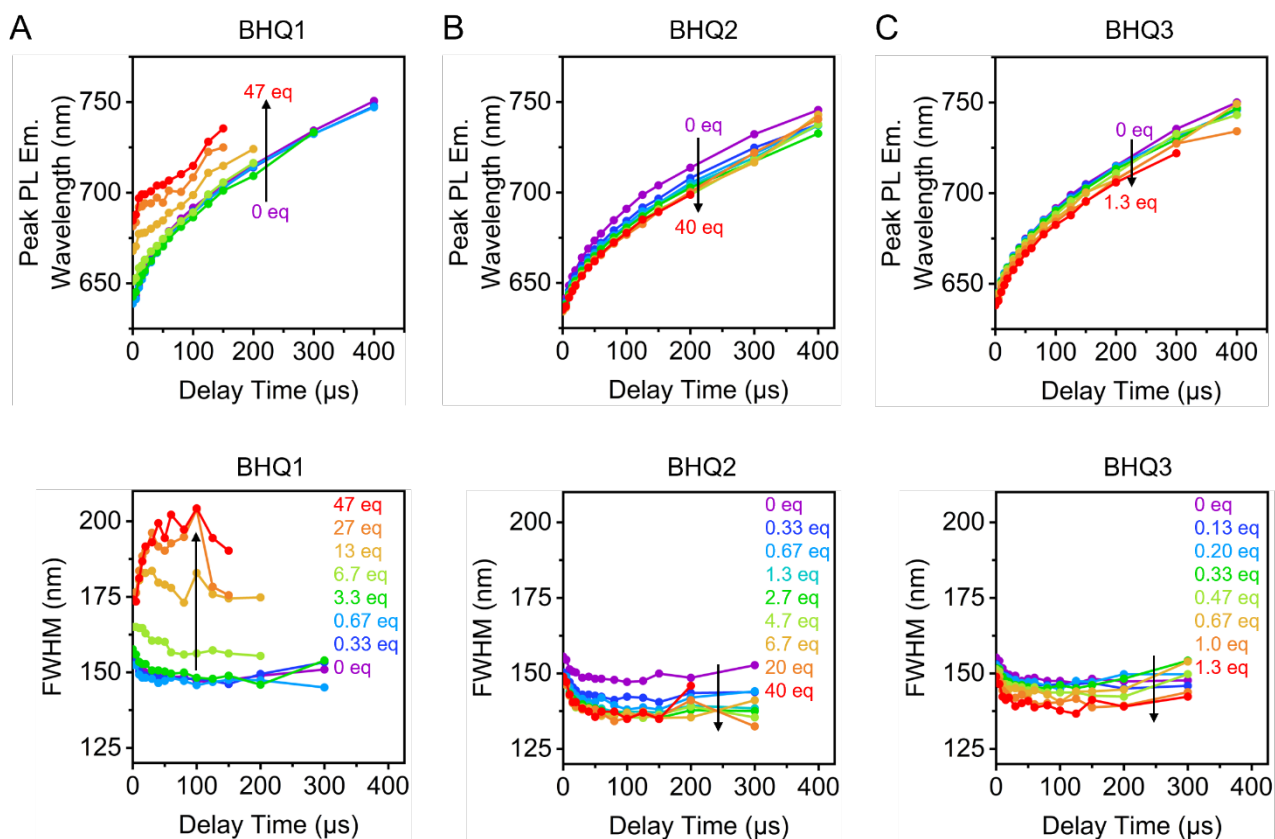
Figure S14. TG spectral snapshots (various delay time, 20 µs integration time) of SiNC676 **1** with partitioned BHQ dyes. **(A)** SiNCs with various equivalents of partitioned BHQ1: (i) emission peak shift versus delay time and (ii) FWHM versus delay time. **(B)** SiNCs with various equivalents of partitioned BHQ2: (i) emission peak shift versus delay time and (ii) FWHM versus delay time. **(C)** SiNCs with various equivalents of partitioned BHQ3: (i) emission peak shift versus delay time and (ii) FWHM versus delay time.

Lastly, the quenching efficiency as a function of wavelength and delay time was evaluated. For BHQ1, the ET efficiency skewed toward higher values at longer wavelengths for lower equivalents of dyes, and toward shorter wavelengths for higher equivalents of dye (Figure S15A). For BHQ3, the quenching efficiency was consistently skewed toward higher values at longer wavelengths (Figure S15C). These overall trends were similar to those observed with prompt ensemble spectra (0 µs delay time, 2 ms integration time, Figure 6C). For BHQ2, the quenching efficiency was consistently skewed toward higher values at longer wavelengths (Figure S15B), similar to the trend in Figure S12B. For BHQ1, BHQ2, and BHQ3, the apparent ET efficiency increased as the delay time increased. This trend likely resulted from ET-induced shortening of the PL lifetime: a sub-population of SiNCs that previously contributed non-zero emission to given "snapshot" time window instead contributed negligible emission.
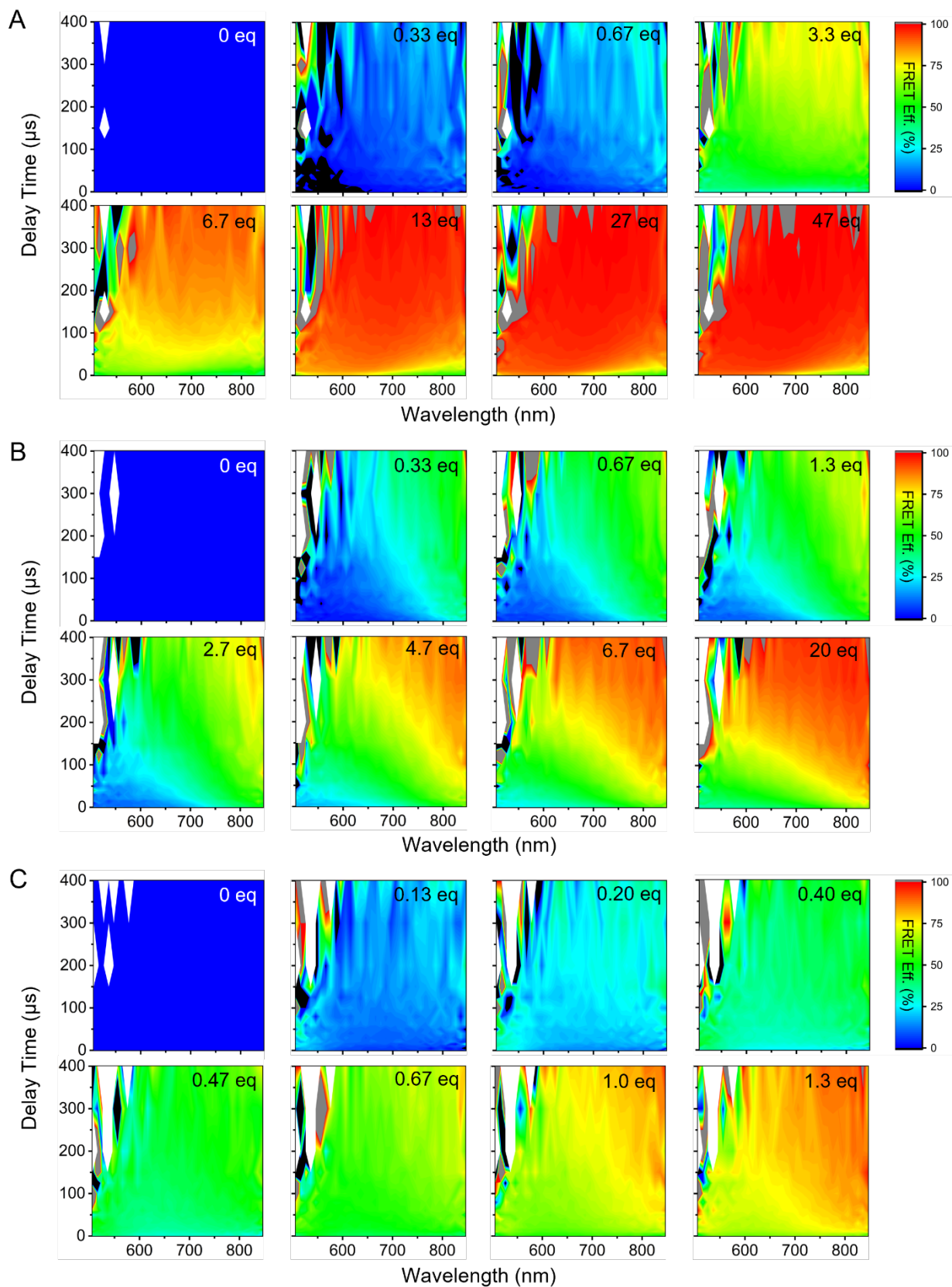
Figure S15. ET efficiency as a function wavelength and delay time (various delay times, 20 μs integration time). SiNC676 **1** partitioned with **(A)** BHQ1, **(B)** BHQ2, and **(C)** BHQ3.

SiNC676 2 with Conjugated BHQ1 and BHQ3 Dyes. Figure S16 shows the absorption spectra of purified samples of SiNC676 **2** conjugated with BHQ1 and BHQ3. The samples were washed with 60% EtOH (*aq*) via 30 kDa centrifugal filters. The excess BHQ was expected to pass through the 30 kDa membrane. The filtrates gradually turned from coloured to nearly colourless after several cycles of washing. The absorption spectra for the purified samples show the absorbance features of BHQ1 and BHQ3, which indicated successful conjugation.
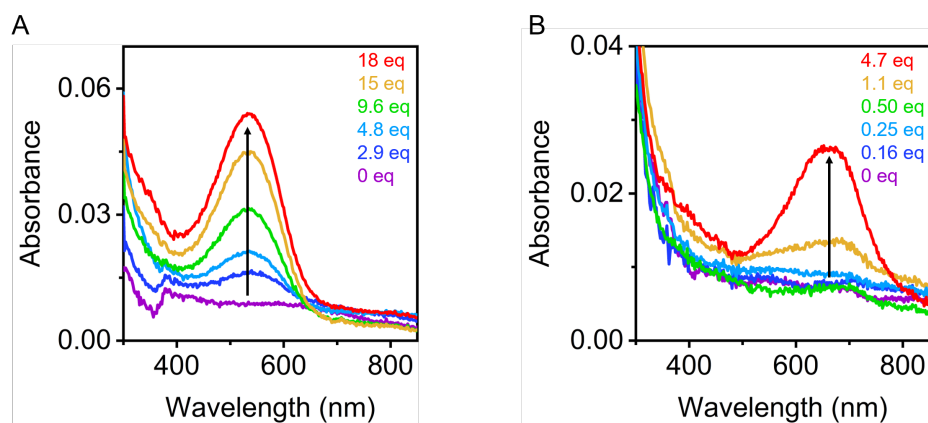

Figure S16. Absorption spectra of SiNC676 **2** with conjugated **(A)** BHQ1 and **(B)** BHQ3, after purification.

Box-car PL lifetime measurements were analyzed for multiple wavelength windows (Figure S17). The lifetime derived from the box-car method were converted to the ET efficiencies plotted in Figure 8C (open points).
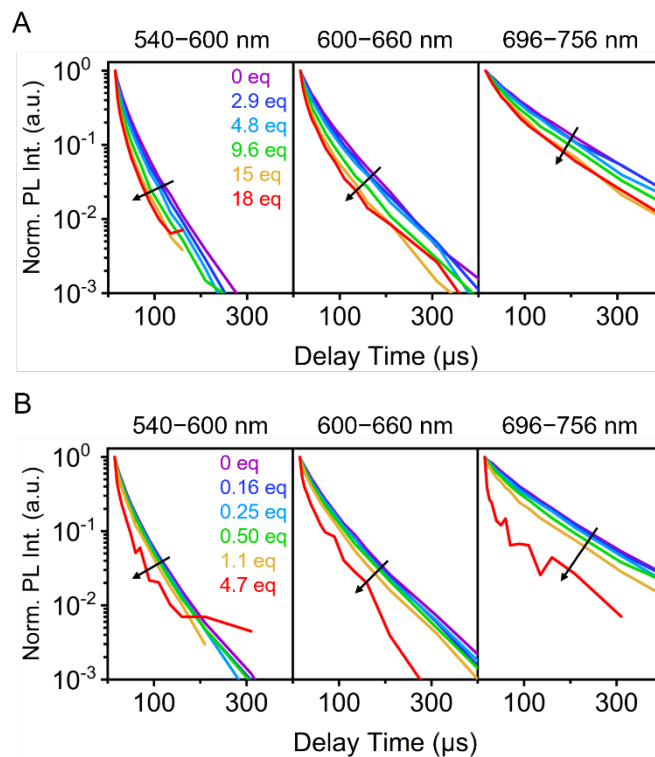
Figure S17. Box-car measurements of SiNC676 **2** with conjugated **(A)** BHQ1 and **(B)** BHQ3 at 540−600 nm, 600−660 nm, and 696−756 nm.

For conjugated BHQ1 and BHQ3 dye, the temporal change in FWHM was much reduced versus the analogous data for partitioned dye (Figure S18). The ET efficiency as a function of wavelength and delay time was evaluated: conjugated BHQ1 and BHQ3 both had higher efficiencies for the shorter wavelength range (Figure S19). As with partitioned dye, the apparent ET efficiency generally increased as the delay time increased (Figure S15), but the magnitudes of these change were smaller.
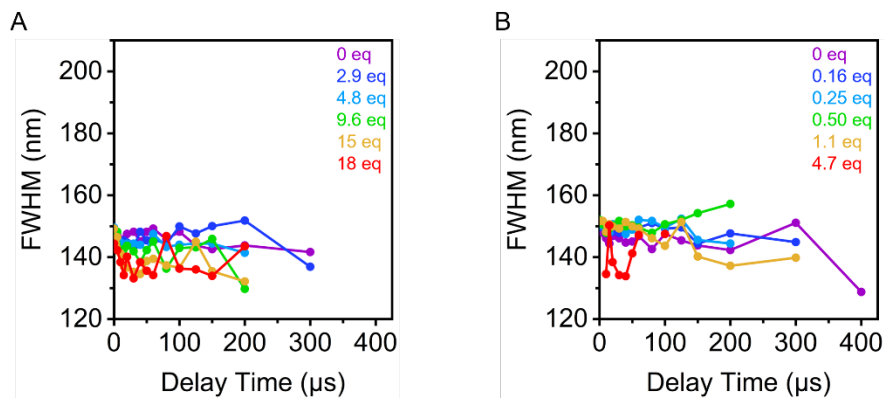

Figure S18. FWHM versus delay time for **(A)** SiNC676 **2** conjugated with various equivalents of BHQ1 and **(B)** SiNC676 **2** conjugated with various equivalents of BHQ3.
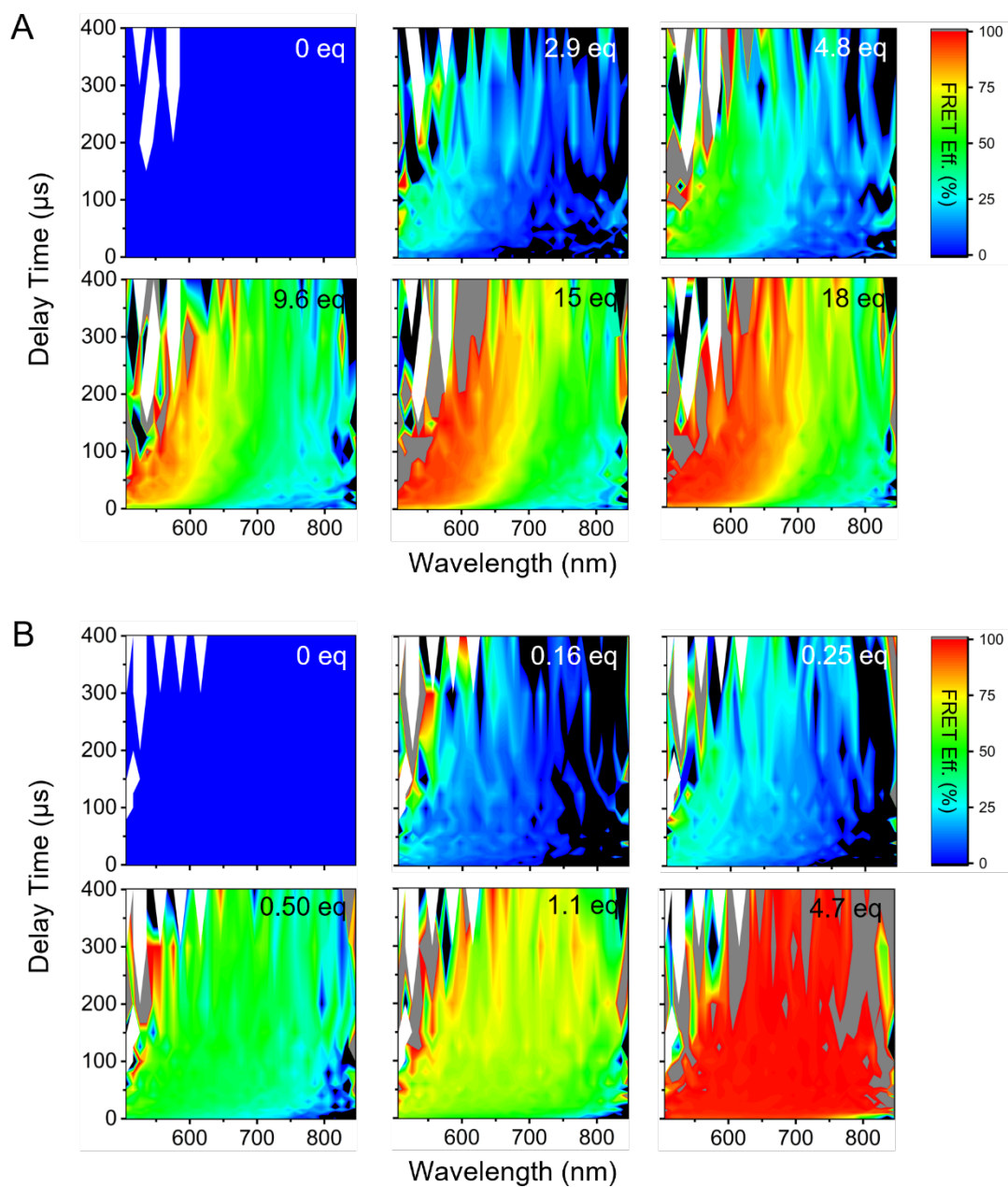
Figure S19. ET efficiency as a function of wavelength and delay time (various delay times, 20 μs integration time) for SiNC676 **2** conjugated with **(A)** BHQ1 and **(B)** BHQ3.

Absorption Spectra for SiNC676 2 Conjugated with sCy5.5. Figure S20 shows the absorption spectra of samples of purified SiNC676 **2** with conjugated sCy5.5. The samples were washed with 1× DPBS via 30 kDa centrifugal filters. The excess sCy5.5 was expected to pass through the 30 kDa membrane. The absorption spectra of the purified samples showed the absorbance feature of sCy5.5, which indicated successful conjugations.
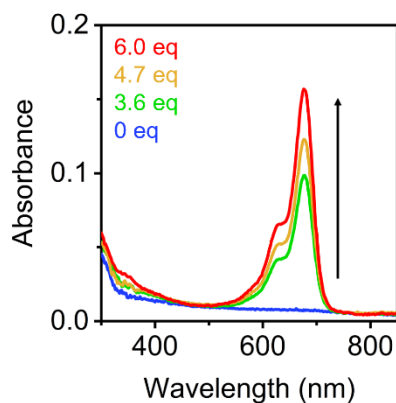
Figure S20. Absorption spectra of SiNC676 **2** with conjugated sCy5.5, after purification.

PL lifetimes derived from box-car PL lifetime measurements in multiple wavelength windows (Figure S21) were converted to the ET efficiencies plotted in Figure 9D (open points), and were consistent with the spectral overlap integrals (Figure 9B).
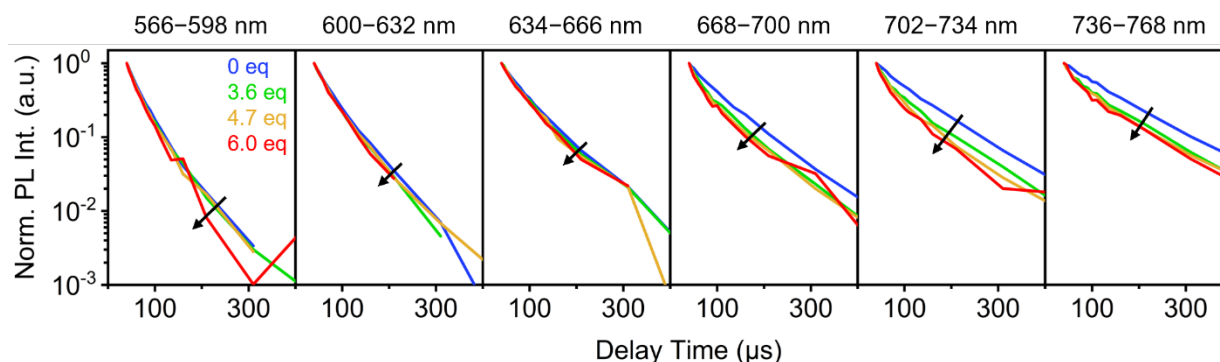
Figure S21. Box-car PL lifetime measurements for SiNC **2** conjugated with sCy5.5 for wavelength ranges of 566−598 nm, 600−632 nm, 634−666 nm, 668−700 nm, 702−734 nm, and 736−768 nm.

Lifetime Data and ET Efficiency. Tables S2−S7 (following pages) summarize PL lifetime fitting parameters and the resulting ET efficiencies. Table S8 summarizes the ensemble ET efficiencies for partitioned samples with estimation via both PL intensity data and TR PL data.

Table S2. Lifetime of SiNC676 **1** partitioned with variable equivalent of BHQ1.

Equiv.	Method	λ Range (nm)	τ_1 (µs)	A_1 (%)	τ_2 (µs)	A_2 (%)	τ_{Avg} (µs)	ET (%)
0	TR	540−756	41.14	80.6	100.0	19.4	52.6	0.0
		540−600	29.73	93.4	94.20	6.64	34.0	0.0
		600−660	43.68	85.9	94.79	14.1	50.9	0.0
		696−756	77.16	77.5	141.7	22.5	91.7	0.0
	Box-car	540−600	7.489	76.2	32.13	23.8	13.3	0.0
		600−660	14.55	52.8	53.38	47.2	32.9	0.0
		696−756	29.38	35.4	101.4	64.6	75.9	0.0
0.33	Box-car	540−600	7.751	75.6	32.00	24.4	13.7	0.0*
		600−660	14.07	54.7	51.90	45.3	31.2	5.2
		696−756	25.83	39.7	97.35	60.3	69.0	9.1
0.67	TR	540−756	37.43	81.7	96.77	18.3	48.3	8.1
		540−600	26.66	91.9	81.12	8.10	31.1	8.6
		600−660	40.96	86.3	92.40	13.7	48.0	5.6
		696−756	64.57	66.4	127.2	33.6	85.6	6.7
0.67	Box-car	540−600	7.857	75.5	32.07	24.5	13.8	0.0*
		600−660	14.04	55.2	51.59	44.8	30.9	6.2
		696−756	24.52	41.2	95.73	58.8	66.4	13
3.3	TR	540−756	32.34	81.2	87.47	18.8	42.7	19
		540−600	23.55	90.3	72.41	9.69	28.3	17
		600−660	35.59	83.1	81.57	16.9	43.4	15
		696−756	44.21	56.0	104.3	44.0	70.7	23
3.3	Box-car	540−600	5.676	83.5	27.85	16.5	9.34	30
		600−660	9.253	66.0	43.34	34.0	20.8	37
		696−756	13.36	55.5	70.26	44.5	38.7	49

6.7	Box-car	540−600	4.779	89.3	25.51	10.7	7.00	48
		600−660	6.694	78.7	38.07	21.3	13.4	59
		696−756	11.15	68.7	60.09	31.3	26.5	65
13	TR	540−756	22.00	83.2	71.96	16.8	30.4	42
		540−600	17.87	88.1	60.74	11.9	23.0	32
		600−660	23.55	80.2	66.75	19.8	32.1	37
		696−756	23.93	78.0	87.99	22.0	38.0	59
13	Box-car	540−600	3.385	96.8	22.78	3.16	4.00	70
		600−660	4.455	93.1	31.98	6.87	6.35	81
		696−756	7.635	83.8	44.11	16.2	13.5	82
27	Box-car	540−600	3.102	98.1	22.02	1.88	3.46	74
		600−660	3.702	96.9	28.96	3.13	4.49	86
		696−756	6.101	89.2	34.77	10.8	9.21	88
47	Box-car	540−600	3.920	95.5	21.87	4.54	4.73	65
		600−660	3.783	96.8	27.67	3.24	4.56	86
		696−756	0.9474	99.0	34.03	0.970	1.27	98

* The ET efficiency was mathematically below 0%.

Table S3. Lifetime of SiNC676 **1** partitioned with variable equivalent of BHQ2.

Equiv.	Method	λ Range (nm)	τ_1 (μs)	A_1 (%)	τ_2 (μs)	A_2 (%)	τ_{Avg} (μs)	ET (%)
0	TR	540−600	26.94	91.1	83.28	8.92	32.0	0.0
		600−660	43.20	84.3	91.24	15.7	50.7	0.0
		696−756	68.81	61.6	124.6	38.4	90.2	0.0
	Box-car	540−600	7.338	75.3	30.89	24.7	13.2	0.0
		600−660	14.47	54.0	52.53	46.0	32.0	0.0
		696−756	32.03	41.3	103.9	58.7	74.2	0.0
0.33	TR	540−600	27.24	91.9	82.50	8.08	31.7	0.82
		600−660	41.93	86.4	92.96	13.6	48.8	3.7
		696−756	55.44	50.0	111.5	50.0	83.5	7.5
0.33	Box-car	540−600	7.965	74.8	31.28	25.2	13.8	0.0*
		600−660	14.58	56.5	50.92	43.5	30.4	5.0
		696−756	24.07	43.5	90.07	56.5	61.4	17
0.67	Box-car	540−600	7.836	75.4	30.91	24.6	13.5	0.0*
		600−660	14.64	56.4	49.99	43.6	30.0	6.1
		696−756	22.14	43.9	84.96	56.1	57.4	23
1.3	Box-car	540−600	7.992	75.0	30.61	25.0	13.7	0.0*
		600−660	14.02	57.3	48.46	42.7	28.7	10
		696−756	20.82	45.6	80.98	54.4	53.5	28
2.7	TR	540−600	27.28	93.8	92.15	6.24	31.3	2.0
		600−660	40.82	86.0	88.28	14.0	47.5	6.4
		696−756	59.21	63.6	115.2	36.4	79.6	12
2.7	Box-car	540−600	8.130	75.5	30.85	24.5	13.7	0.0*
		600−660	14.93	58.9	49.35	41.1	29.1	9.1
		696−756	19.48	44.3	77.61	55.7	51.9	30
4.7	Box-car	540−600	7.562	76.6	29.13	23.4	12.6	4.2
		600−660	13.67	58.8	45.02	41.2	26.6	17
		696−756	17.19	48.1	69.17	51.9	44.1	41
6.7	TR	540−600	25.93	94.6	90.39	5.43	29.4	8.0
		600−660	37.49	87.7	83.02	12.3	43.1	15

		696−756	47.43	69.1	105.4	30.9	65.4	28
6.7	Box-car	540−600	7.974	75.6	28.63	24.4	13.0	1.1
		600−660	13.09	59.2	42.83	40.8	25.2	21
		696−756	13.56	47.6	60.86	52.4	38.4	48
20	Box-car	540−600	6.480	78.4	25.71	21.6	10.6	19
		600−660	10.39	58.0	37.09	42.0	21.6	32
		696−756	11.68	51.3	53.80	48.7	32.2	57
40	Box-car	540−600	6.520	77.8	24.69	22.2	10.6	20
		600−660	9.527	59.5	34.83	40.5	19.8	38
		696−756	10.59	55.2	49.94	44.8	28.2	62

* The ET efficiency was below 0%.

Table S4. Lifetime of SiNC676 **1** partitioned with variable equivalent of BHQ3.

Equiv.	Method	λ Range(nm)	τ_1 (μs)	A_1 (%)	τ_2 (μs)	A_2 (%)	τ_{Avg} (μs)	ET (%)
0	TR	540−756	42.33	80.6	103.4	19.4	54.2	0.0
		540−600	28.65	91.6	85.42	8.44	33.4	0.0
		600−660	44.91	85.9	96.08	14.1	52.1	0.0
		696−756	73.09	60.0	126.0	40.0	94.3	0.0
	Box-car	540−600	8.031	74.3	32.92	25.7	14.4	0.0
		600−660	15.33	51.8	54.03	48.2	34.0	0.0
		696−756	31.85	37.1	103.1	62.9	76.7	0.0
0.13	Box-car	540−600	7.479	76.8	32.37	23.2	13.2	8.2
		600−660	13.19	54.2	51.45	45.8	30.7	9.7
		696−756	23.37	35.1	90.98	64.9	67.3	12
0.20	TR	540−756	45.43	82.1	105.4	17.9	56.2	0.0*
		540−600	28.35	91.5	85.19	8.51	33.2	0.8
		600−660	46.08	84.5	90.39	15.5	53.0	0.0*
		696−756	76.20	72.7	130.6	27.3	91.1	3.4
0.20	Box-car	540−600	7.535	76.7	32.60	23.3	13.4	7.4
		600−660	12.47	54.4	50.26	45.6	29.7	13
		696−756	21.74	37.3	90.22	62.7	64.7	16
0.33	Box-car	540−600	7.250	77.7	31.73	22.3	12.7	12
		600−660	11.83	57.1	49.69	42.9	28.1	17
		696−756	16.19	39.1	83.92	60.9	57.4	25
0.47	Box-car	540−600	6.503	79.9	30.82	20.1	11.4	21
		600−660	11.97	58.0	49.74	42.0	27.8	18
		696−756	14.75	41.0	81.22	59.0	54.0	30
0.67	TR	540−756	35.38	81.4	93.8	18.6	46.3	15
		540−600	22.36	89.8	71.47	10.2	27.4	18
		600−660	37.23	82.4	84.62	17.6	45.6	13
		696−756	50.35	52.0	109.6	48.0	78.8	16
0.67	Box-car	540−600	6.790	80.6	31.23	19.4	11.5	20
		600−660	11.13	60.6	48.42	39.4	25.8	24

		696−756	11.42	46.8	76.30	53.2	45.9	40
1.0	Box-car	540−600	6.383	82.6	30.10	17.4	10.5	27
		600−660	10.13	63.8	46.72	36.2	23.4	31
		696−756	11.96	51.0	74.67	49.0	42.7	44
1.3	TR	540−756	26.33	78.5	81.2	21.5	38.1	30
		540−600	16.52	88.2	59.90	11.8	21.7	35
		600−660	32.22	79.7	78.31	20.3	41.6	20
		696−756	44.10	55.2	106.9	44.8	72.3	23
1.3	Box-car	540−600	6.002	84.4	29.18	15.6	9.61	33
		600−660	8.713	66.8	44.10	33.2	20.5	40
		696−756	9.611	59.8	70.95	40.2	34.3	55

* The ET efficiency was below 0%.

Table S5. Lifetime of SiNC676 **2** conjugated with variable equivalent of BHQ1.

Equiv.	Method	λ Range (nm)	τ_1 (µs)	A_1 (%)	τ_2 (µs)	A_2 (%)	τ_{Avg} (µs)	ET (%)
0	Box-car	540−600	8.345	38.1	31.72	61.9	22.8	0.0
		600−660	18.20	41.5	57.35	58.5	41.1	0.0
		696−756	37.91	35.1	117.5	64.9	89.6	0.0
2.9	Box-car	540−600	7.441	45.0	30.37	55.0	20.0	12
		600−660	14.87	44.0	53.87	56.0	36.7	11
		696−756	29.27	29.0	99.46	71.0	79.1	12
4.8	Box-car	540−600	6.544	47.9	28.66	52.1	18.1	21
		600−660	12.09	41.3	48.23	58.7	33.3	19
		696−756	33.69	39.9	111.1	60.1	80.2	10
9.6	Box-car	540−600	4.396	51.5	23.57	48.5	13.7	40
		600−660	7.946	42.6	39.31	57.4	25.9	37
		696−756	25.40	38.5	94.66	61.5	68.0	24
14.9	Box-car	540−600	3.187	55.8	20.32	44.2	10.8	53
		600−660	6.148	48.9	34.74	51.1	20.7	50
		696−756	16.23	37.6	80.76	62.4	56.5	37
17.8	Box-car	540−600	3.086	59.9	19.42	40.1	9.63	58
		600−660	5.576	52.8	32.34	47.2	18.2	56
		696−756	20.47	45.6	81.83	54.4	53.9	40

Table S6. Lifetime of SiNC676 **2** conjugated with variable equivalent of BHQ3.

Equiv.	Method	λ Range (nm)	τ_1 (µs)	A_1 (%)	τ_2 (µs)	A_2 (%)	τ_{Avg} (µs)	ET (%)
0	Box-car	540−600	10.54	41.3	35.97	58.7	25.5	0.0
		600−660	22.23	42.4	61.39	57.6	44.8	0.0
		696−756	51.85	45.5	128.2	54.5	93.4	0.0
0.16	Box-car	540−600	8.754	40.0	34.65	60.0	24.3	4.6
		600−660	14.82	31.8	54.51	68.2	41.9	6.5
		696−756	20.97	19.0	98.13	81.0	83.4	11
0.25	Box-car	540−600	8.138	38.1	33.18	61.9	23.6	7.2
		600−660	14.85	36.7	56.14	63.3	41.0	8.5
		696−756	23.34	26.2	101.2	73.8	80.9	13
0.50	Box-car	540−600	8.034	40.7	32.78	59.3	22.7	11
		600−660	13.66	37.9	52.98	62.1	38.1	15
		696−756	20.05	27.8	89.38	72.2	70.1	25
1.1	Box-car	540−600	5.157	37.4	27.94	62.6	19.4	24
		600−660	8.217	33.7	45.18	66.3	32.7	27
		696−756	8.827	26.1	68.53	73.9	53.0	43
4.7	Box-car	540−600	2.594	52.2	20.47	47.8	11.1	56
		600−660	0.01893	50.9	38.19	49.1	18.8	58
		696−756	2.904	70.9	40.65	29.1	13.9	85

Table S7. Lifetime of SiNC676 **2** conjugated with variable equivalent of sCy5.5.

Equiv.	Method	λ Range (nm)	τ_1 (µs)	A_1 (%)	τ_2 (µs)	A_2 (%)	τ_{Avg} (µs)	ET (%)
0	Box-car	566−598	17.89	62.5	45.66	37.5	28.3	0.0
		600−632	24.83	60.2	61.20	39.8	39.3	0.0
		634−666	27.48	46.6	72.28	53.4	51.4	0.0
		668−700	24.72	36.2	85.18	63.8	63.3	0.0
		702−734	45.52	50.3	134.8	49.7	89.9	0.0
		736−768	22.35	11.5	114.2	88.5	104	0.0
3.6	Box-car	566−598	16.99	72.8	47.76	27.2	25.4	10
		600−632	14.80	51.7	47.83	48.3	30.7	22
		634−666	23.91	56.5	71.21	43.5	44.5	13
		668−700	17.72	68.7	81.63	31.3	37.7	40
		702−734	16.66	67.6	89.05	32.4	40.1	55
		736−768	14.81	63.3	101.7	36.7	46.7	55
4.7	Box-car	566−598	15.14	66.6	42.05	33.4	24.1	15
		600−632	27.20	79.4	74.95	20.6	37.0	5.8
		634−666	25.11	57.1	70.36	42.9	44.5	13
		668−700	14.10	76.9	75.05	23.1	28.2	55
		702−734	13.06	69.5	69.00	30.5	30.1	66
		736−768	14.68	65.4	95.06	34.6	42.5	59
6.0	Box-car	566−598	11.04	68.3	36.56	31.7	19.1	32
		600−632	18.70	58.7	52.35	41.3	32.6	17
		634−666	14.12	55.1	60.20	44.9	34.8	32
		668−700	10.95	81.0	62.85	19.0	20.8	67
		702−734	12.81	80.1	72.30	19.9	24.7	73
		736−768	23.91	73.2	132.6	26.8	53.1	49

Table S8. ET efficiencies for SiNC676 **1** partitioned with various equivalents of BHQ1 and BHQ3 dyes, estimated from PL intensity data and TR PL data.

Dye	Equiv.	ET (PL Int.) (%)	ET (TR) (%)
BHQ1	0	0.0	0.0
	0.67	4.9	8.1
	3.3	46	19
	13	83	42
BHQ3	0	0.0	0.0
	0.20	15	0.0*
	0.67	49	15
	1.3	70	30

* The ET efficiency was below 0%.

The wavelength ranges were 500–850 nm for PL intensity data and 540–756 nm for TR PL data.

Additional Discussion of Limitations of this Study. SiNCs, whether paired with BHQ dyes or fluorescent sCy5.5 dyes, are a challenging system for studying ET. This section expands on the discussion of some of the challenges and limitations associated with SiNCs as donor materials, our experiments, and the interpretation of data and results.

Acceptor/Donor Ratios

Dye concentrations are straightforward to determine with their well-defined absorption peaks, their well-known molar absorption coefficients, and the expectation of a Poisson-like distribution of dyes per SiNC. The challenge is obtaining an accurate concentration of SiNCs. Although non-optical methods (*e.g.,* combination of TEM and TGA) may be used to estimate the concentration of a batch of material, the methods tend to be impractical for the scale of individual samples. Optical absorbance methods are far more suitable, but are limited by the relatively weak absorption of the SiNC and lack of defined peak—especially in comparison to dyes within the same sample. An advantage of the partitioning approach with BHQ dyes was that it did not require purification after adding dye, thereby avoiding potential loss of SiNCs during purification. In turn, this benefit enabled more reliable measurements of ET efficiency from quenching of the SiNC PL and more precise variation of the relative amount of dye per SiNC.

To assess the plausibility of the initial estimate of the SiNC concentration, we started from the limiting hypothesis that one BHQ3 was able to quench one SiNC with 100% ET efficiency. With a Poisson distribution of one dye per SiNC, ~63% of the SiNC population would have $\geq$ 1 BHQ3 molecule. In our prompt ensemble measurements, a putative 0.15 equivalents of BHQ3 FRET yielded ~63% quenching, which indicated that the actual SiNC concentration was at least 6.7-fold more dilute than the initial estimate (*vide supra* for method). Of course, it is also possible that one SiNC requires more than one BHQ3 for complete quenching, which would suggest an even larger correction. The values for the number of equivalents of dye were therefore revised from the initial concentration estimates by 6.7-fold, yielding the numbers reported in all figures, as well as calculated donor-acceptor distances that were longer and more consistent with the expected nanocrystal radii plus coating thickness.

Orientation Factor

Another limitation is the assumption that the orientation factor was $\kappa^2 = 2/3$, corresponding to dynamically random orientations of the SiNC and dye transition dipoles, when calculating the Förster distances. This assumption has generally proven adequate with CdSe QDs and is plausible for conjugated hydrophilic sCy5.5. However, for all the hydrophobic BHQ dyes, which have a preference to partition into the SiNC surface coating, the assumption of dynamic rotation is questionable. Nevertheless, any error in the κ^2 should apply across the ensemble of SiNCs, affecting the R_0 for different sub-populations by the same relative degree. The observed qualitative trends should not be significantly affected by the assumption of $\kappa^2 = 2/3$.

Inner Filter Effects

A final limitation to consider is inner filter effects. Intensity measurements yielded higher ET efficiencies than lifetime measurements and inner filter effects are a possible explanation for this difference. However, our checks suggested an absence of significant inner filter effects (*vide supra* for data). The occurrence of ET also remained clear from the dye-induced decrease in SiNC PL lifetime and from the observation of sCy5.5 PL emission that, due to time-gating, must have arose from ET rather than direct excitation. As noted in the main text, there was also another explanation for the discrepancy between intensity-derived and lifetime-derived ET efficiencies: specifically, the occurrence of high-efficiency ET with unresolvably short PL lifetimes and/or quenched PL intensities for certain sub-populations of SiNCs. Nevertheless, a minor contribution from inner filter effects cannot be completely ruled out. Given their relatively weak absorption compared to many organic dyes, inner filter effects are likely something that will need to be consistently guarded against for ET studies with SiNCs.

Supplemental References

1   C. J. T. Robidillo, M. A. Islam, M. Aghajamali, A. Faramus, R. Sinelnikov, X. Zhang, J. Boekhoven and J. G. C. Veinot, *Langmuir*, 2018, **34**, 6556–6569.

2   S. L. Anderson, E. J. Luber, B. C. Olsen and J. M. Buriak, *Chem. Mater.*, 2016, **28**, 5973–5975.

3   H. Kim, T. Jeen, M. V. Tran and W. R. Algar, *Analyst*, 2018, **143**, 1104–1116.

4   K. D. Krause, H.-Y. Tsai, K. Rees, H. Kim and W. R. Algar, in *Peptide Conjugation: Methods and Protocols*, ed. W. M. Hussein, R. J. Stephenson and I. Toth, Humana New York, NY, 1st edn., 2021, ch.16, pp. 175–218.

5   W. R. Algar, M. G. Ancona, A. P. Malanoski, K. Susumu and I. L. Medintz, *ACS Nano*, 2012, **6**, 11044–11058.

6   J. J. Li and W. R. Algar, *Analyst*, 2016, **141**, 3636–3647.

7   L. Porrès, A. Holland, L.-O. Pålsson, A. P. Monkman, C. Kemp and A. Beeby, *J. Fluoresc.*, 2006, **16**, 267–273.

8   A. M. Brouwer, *Pure Appl. Chem.*, 2011, **83**, 2213–2228.